Design of a Series-Elastic Actuator for a Humanoid Robot for Space Applications

Shubhankar Riswadkar
IGMR
RWTH AACHEN University
Aachen, Germany
riswadkar@igmr.rwth-aachen.de

S Barat
Mechanical Engineering
IIT GANDHINAGAR
Gandhinagar, India
barats@iitgn.ac.in

Harish Palanthandalam Madapusi
Mechanical Engineering
IIT GANDHINAGAR
Gandhinagar, India
harish@iitgn.ac.in

***Abstract*—Robots in space operate in highly unstructured environments and terrains due to which compliant actuators are preferred over rigid geared actuators. Series Elastic Actuators (SEAs) are a common choice for compliant actuation as they protect both the robot and the environment from unexpected collisions. The low output impedance due to the integration of a passive compliance element makes it capable of effective stable interactions with the environment. This paper describes the development of the Series Elastic Actuator (SEA) for space application through key considerations such as transparency, torque tracking bandwidth, and impedance rendering.**

***Index Terms*—SEA, impedance, transparency, torque tracking, compliance, stiffness**

I. Introduction

In space applications, a humanoid robot is required to assist the crew in carrying out maintenance and extraterrestrial missions where the environment is far from structured. In past missions, on-site structure and robot interfaces have been used for improving compatibility for robot assistance, it cannot meet all the assistance and service requirements. Conventionally, compliance has been added as a part of the control architecture, in the form of impedance control [1] or stiffness control but hardware limitations like computational delay, backlash, and nonlinearity of actuators still pose a challenge to safe interaction in contact tasks. Pratt and Williamson first introduced Series Elastic Actuators (SEAs) in [2] as an interface to adjust the stiffness between the actuator and its load. Although the introduction of the compliance element between the actuator and the load lowers the closed-loop bandwidth for position and torque control it offers many advantages such as the ability to render impedance as required, greater shock tolerance, lower inertia, and so on [3]. As compared to geared actuators, the introduction of the compliance element also provides feedback on the force applied at the joint through the measurement of angular deflection, essentially transforming the force control problem into a position control one. This property of the SEAs has led to their use in 25 out of 44 degrees of freedom (dof) in NASA's Valkyrie Robot [4]. Energy storage in the SEAs has also led to improved efficiency and better shock protection as impacts occur in every step in legged robots [5]. SEAs also make it possible to design custom torsion springs that provide sufficiently high stiffness in a compact size which are easily integrated with the geared actuator as seen in NASA's Robonaut 2 (R2) [6]. This paper provides details on designing a SEA that has a requirement of nominal torque to be around 15 N m, speed of 10-12 rpm, and a backdrivable torque of less than 2 N m. This paper summarizes well-established properties of the SEA for the design of an actuator for humanoid robots in space through simulations and experimental results.

II. Modelling

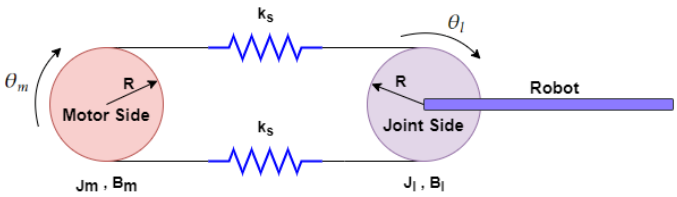

Fig. 1. Schematic representation of Linear spring based SEA

Fig 1 represents the schematic representation of a SEA for control design purposes. A robotic joint has been coupled to a DC motor called the motor side via two linear springs. The springs compress and extend, delivering torque to the robotic joint connected to a link. We assume clockwise positive for angular displacements $\theta_1 = \frac{\theta_m}{r}$ and θ_l. The equations of motion can be derived as follows

$$r\tau_m = J_{eq}\ddot{\theta}_1 + B_{eq}\dot{\theta}_1 + 2k_sR^2(\theta_1 - \theta_l), \tag{1}$$

$$\tau_l = J_l\ddot{\theta}_l + B_l\dot{\theta}_l - 2k_sR^2(\theta_1 - \theta_l). \tag{2}$$

where, $J_{eq} = J_g + J_m r^2$ and $B_{eq} = B_g + B_m r^2$. Here, the subscript m, g, and l denote the motor, gearbox, and external load sides, respectively. k_s, r, R, J, B, θ denote the spring constant, gear ratio, pulley radius, inertia, viscous damping, and angular displacement respectively. Taking the Laplace transform, and the external applied load torque $\tau_l = 0$ we can rewrite (1) and (2) as the open-loop position transfer function,

$$\frac{\theta_l}{\theta_m} = \frac{2k_sR^2}{(J_ls^2 + B_ls + 2k_sR^2)r}. \tag{3}$$

Next, it follows that in the absence of an externally applied load torque, the only torque being delivered to the joint side is the spring torque τ_k

$$\tau_k(s) = 2k_sR^2(\theta_1(s) - \theta_l(s)). \tag{4}$$

(3) and (4) can be used to rewrite (1) and (2) as the open-loop torque transfer function as

$$\frac{\tau_k(s)}{\tau_m(s)} = \frac{c_0 s^2 + c_1 s}{d_0 s^4 + d_1 s^3 + d_2 s^2 + d_3 s} \tag{5}$$

where, $c_0 = 2k_s R^2 J_l r$, $c_1 = 2k_s R^2 B_l r$, $d_0 = J_l J_{eq}$, $d_1 = (J_l B_{eq} + B_l J_{eq})$, $d_2 = 2k_s R^2 (J_{eq} + J_l) + B_l B_{eq}$, $d_3 = 2k_s R^2 (B_{eq} + B_l)$. Taking $\Delta\theta(s) = \theta_1(s) - \theta_l(s)$ as the angular deflection between the motor and joint side pulleys, we can rewrite (1)

$$r\tau_m(s) = (J_{eq} s^2 + B_{eq} s)\theta_l(s) + (J_{eq} s^2 + B_{eq} s + 2k_s R^2)\Delta\theta(s)). \tag{6}$$

Considering the equation of the feedback controller as $C(s) = K_p + K_d s$ (PD control), we get

$$\tau_m(s) = C(s)(\tau_d(s) - 2k_s R^2 \Delta\theta(s)) + \lambda(s)\tau_d(s). \tag{7}$$

Here $\lambda(s)\tau_d(s)$ is the feedforward term which has been added to eliminate the steady-state error. (6) and (7) can be rearranged to give two new closed-loop transfer functions as

$$\frac{\tau_k(s)}{\theta_l(s)} = \frac{-2k_s R^2 (J_{eq} s^2 + B_{eq} s)}{J_{eq} s^2 + B_{eq} s + 2k_s R^2 (1 + K_p + K_d s) r}. \tag{8}$$

$$\frac{\tau_k(s)}{\tau_d(s)} = \frac{2k_s R^2 (K_p + K_d s + 1) r}{J_{eq} s^2 + B_{eq} s + 2k_s R^2 (1 + K_p + K_d s) r}. \tag{9}$$

(8) is known as the transparency of the SEA and (9) as the torque tracking transfer function. These two transfer functions completely define the closed-loop characteristics of the SEA. For more details on the derivation please refer to [7].

III. Control Architecture

Using a torque-sourced SEA, where the electric motor is used as a torque source see Fig 2 has been the conventional practice in ensuring that the actuator can quickly deliver the required torque to the load side to have good control over the robot joint as seen in [7].

However, a new approach has been presented in [8], highlighting a newer control strategy, using the motor as a velocity source see Fig 3. A tight velocity control loop can overcome some undesirable effects of the motor and gearbox such as stiction, non-linear effects which cannot be accounted for in modeling, etc. Additionally, it is easier to implement velocity control for the motor than current control. If we think on a more fundamental level, tasks that require Force or Impedance Control, the inherent velocity of the motor itself is low, due to which we can ignore the back-EMF of the motor. In this case, the first order approximation $\frac{i(s)}{V(s)} = \frac{1}{Ls+R}$ is valid. Thus, for tasks in which we require Force or Impedance control, using the motor as a torque source is easier as we can implement current control.

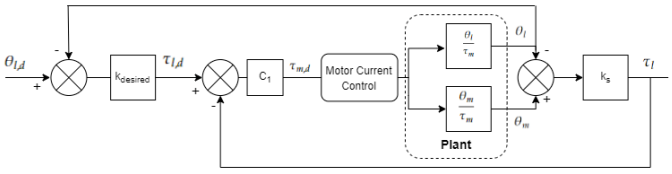

Fig. 2. Joint Stiffness Control of torque sourced SEA

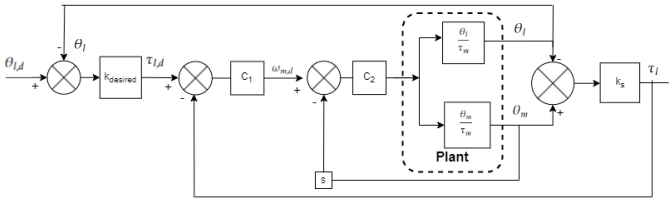

Fig. 3. Joint Stiffness Control of velocity sourced SEA

IV. Simulation Study

A. Transparency

Transparency is defined as the ability to track zero torque in the presence of output load motion. It is the inverse of the residual torque given an imposed output motion. In Fig 1, if the robot link undergoes a motion of θ_l, then transparency is the ability to feel zero torque at the joint. Thus, to feel zero torque at the joint, the springs must provide a compensation torque proportional to the torque due to output motion. At lower frequencies, the actuator has a higher transparency, as (8) $\rightarrow 0$ when $\omega \rightarrow 0$. At higher frequencies, the transparency is upper bounded by the stiffness element. Thus, at lower frequencies, the closed-loop poles dictate the transparency of the actuator, as it is possible to place the closed-loop poles of the transparency transfer function at an arbitrarily high frequency with appropriate gains, while at higher frequencies the stiffness element bounds the transparency of the actuator. Therefore, increasing the stiffness decreases transparency (Fig 4). Fig 5 shows the transparency analysis of SEA in the

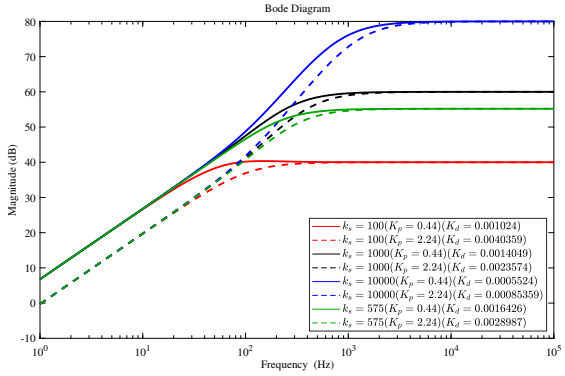

Fig. 4. Simulation results: Effect of varying k_s and K_p and K_d

time domain. An external disturbance torque, sinusoidal in nature of amplitude 1N m is applied to the joint side, and the residual torque delivered at the joint is approximately zero. This satisfies the zero torque tracking ability of the SEA in the presence of load motion. As the spring torque is the only

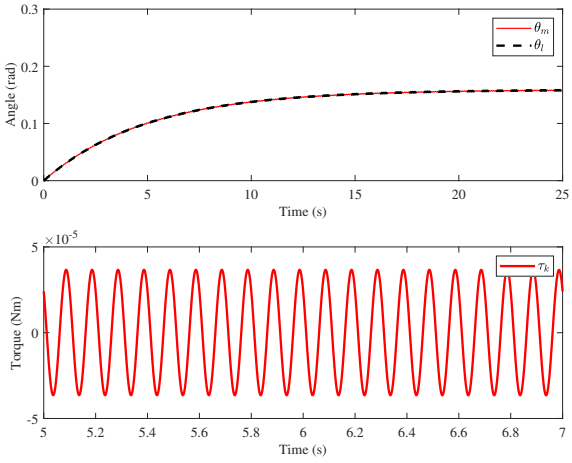

Fig. 5. Simulation results: Transparency of the SEA in time domain

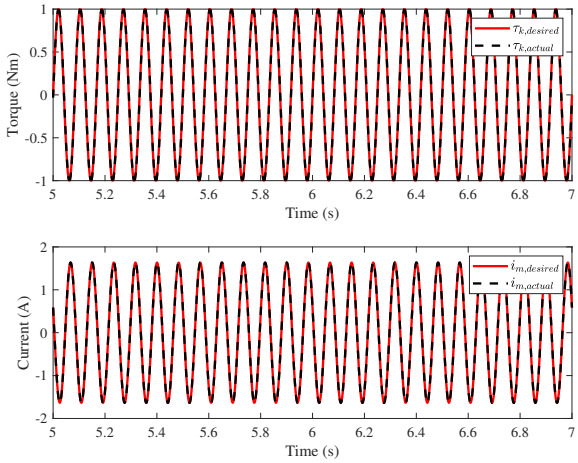

Fig. 7. Simulation results: Torque tracking of SEA in time domain

torque delivered at the joint side, it can only approach zero when $\theta_m \rightarrow \theta_l$

B. Torque Tracking

Increasing the stiffness increases the torque tracking bandwidth as seen in Fig 6. The denominator for (9) is the same as (8). Thus, the same procedure for tuning the closed loop poles can be followed. However, the gains also affect the zeros of (9). Fig 7 shows the tracking of a reference sinusoidal torque input of amplitude 1N m and frequency 12 Hz.

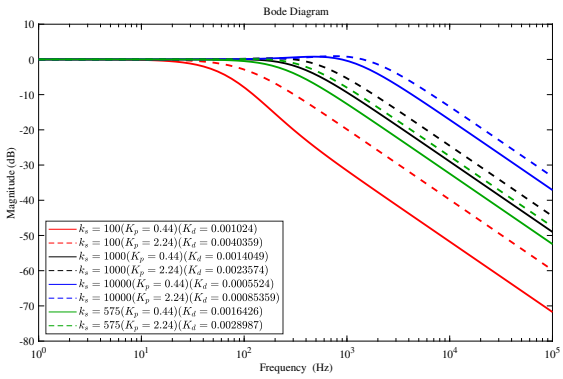

Fig. 6. Simulation results: Effect of varying k_s and K_P and K_d

C. Impedance Rendering

The desired torque is given by,

$$\tau_d(s) = K(\theta_l^d - \theta_l) + D(\dot{\theta_l^d} - \dot{\theta_l}) \tag{10}$$

For the moment, taking $\theta_l^d \equiv \dot{\theta_l^d} \equiv 0$.

$$\tau_d(s) = -(K + Ds)\theta_l(s) \tag{11}$$

Substituting (11) in (7) and reformulating (1), (2) we get the impedance transfer function as,

$$Z(s) = \frac{\tau_k(s)}{\theta_l(s)} = \frac{b_0 s^2 + b_1 s + b_2}{a_0 s^2 + a_1 s + a_2} \tag{12}$$

where $b_0 = -2k_s R^2((J_{eq} + K_d D))$, $b_1 = (B_{eq} + KK_d + D(K_p + 1))$, $b_2 = K(K_p + 1)$, $a_0 = J_{eq}$, $a_1 = B_{eq}$, $a_2 = 2k_s R^2(1 + K_p + K_d s)r$

From (12), it is clear that both torque tracking bandwidth and the transparency of the actuator can limit the range of rendered impedances. For lower stiffness actuators, the torque tracking bandwidth limits the impedance rendering capability of the actuator. This is evident from (12), that at higher frequencies, $s \rightarrow \infty$ magnitude of (12) is upper bounded by,

$$Z(s) = \frac{2k_s R^2(J_{eq} + K_d D)}{J_{eq}} \tag{13}$$

Thus, we can see that at higher frequencies, the actuator's stiffness plays an important role in determining the impedance rendering capability of the actuator as all the other terms are constants. For higher stiffness actuators, the transparency of the actuator upper bounds the value of the rendered impedance as is evident from (13).

V. Experimental Results

The experimental setup consists of a DC motor with a gearbox used as a torque source coupled through linear springs to move a robot link connected to the joint side. The DC motor is controlled using NI SbRIO-9627 with LabVIEW FPGA. The stiffness of the linear springs is around 600N m. CUI AMT-132 quadrature capacitive incremental encoders are used to get the angular position feedback from the motor and joint side. The linear springs are preloaded and they extend and compress to create the required spring torque to be passed to the joint side, and can be easily replaced once they undergo plastic deformation. A small ball is attached to the link to add inertia to the link which makes the position control of the SEA easier as it adds some load on the motor due to which current control of the DC motor becomes possible with ACS 712 current sensor. A PI controller is used for the outer level position controller of the SEA which passes a desired current to the cascaded current controller of the DC motor.

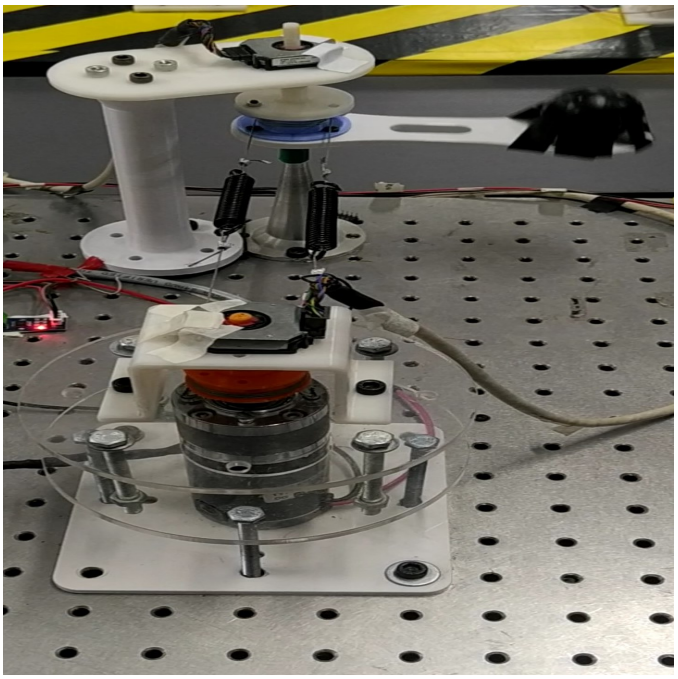

Fig. 8. Hardware test setup

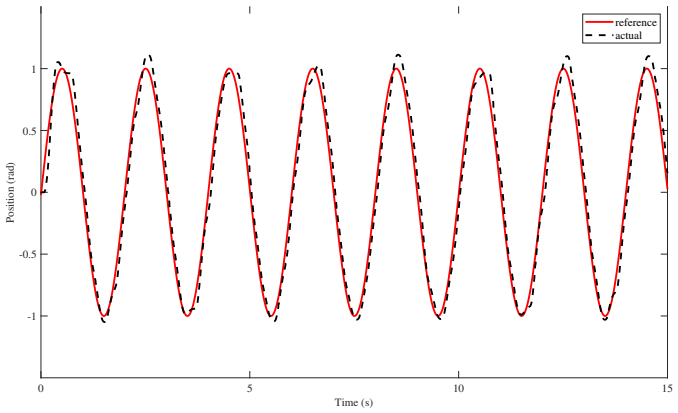

Fig. 9. Experimental position control of SEA tracking a sinusoidal reference of frequency 0.5 Hz and amplitude 1 rad

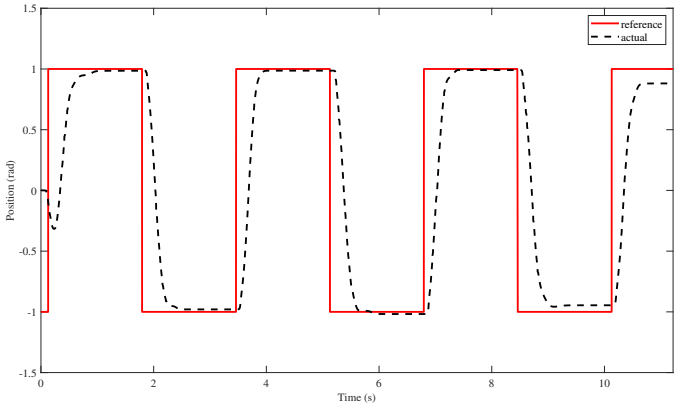

Fig. 10. Experimental position control of SEA tracking a square wave of frequency 0.3 Hz and amplitude 1 rad

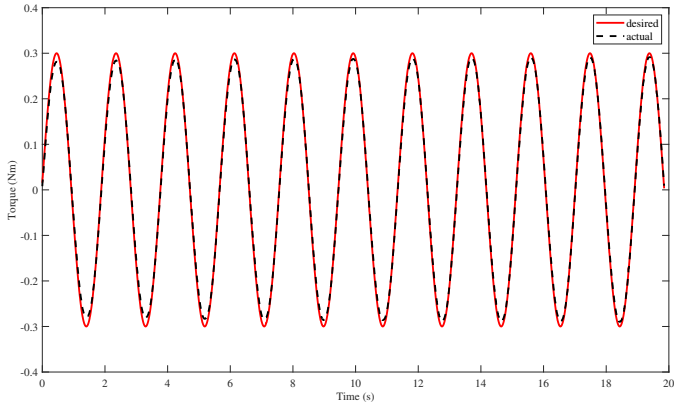

Fig. 11. Experimental torque control of SEA tracking a sinusoidal reference of frequency 0.5 Hz and amplitude 0.3 Nm

Acknowledgment

The authors gratefully acknowledge support for this work from ISRO RESPOND project number ISRO/RES/3/879/21-22. The authors also gratefully acknowledge technical inputs from Mr. Ravichandran and Mrs. Smitha Krishnan from IISU, ISRO as focal points in this project.

VI. Conclusion

The SEA model includes two key transfer functions: transparency and torque tracking, both analyzed via simulation. Increasing the SEA's stiffness improves torque tracking bandwidth but reduces transparency. At lower frequencies, the SEA accurately renders impedance, controlled by the PD controller's effect on the closed-loop poles. Experimental data showed effective position and torque control of the SEA, demonstrated by tracking sine and square waves within its closed-loop bandwidth.

References

[1] N. Hogan, "Impedance Control: An Approach to Manipulation," 1984 American Control Conference, San Diego, CA, USA, 1984, pp. 304-313, doi: 10.23919/ACC.1984.4788393.

[2] G. A. Pratt and M. M. Williamson, "Series elastic actuators," Proceedings 1995 IEEE/RSJ International Conference on Intelligent Robots and Systems. Human Robot Interaction and Cooperative Robots, Pittsburgh, PA, USA, 1995, pp. 399-406 vol.1, doi: 10.1109/IROS.1995.525827.

[3] Y. Zhao, N. Paine, S. J. Jorgensen and L. Sentis, "Impedance Control and Performance Measure of Series Elastic Actuators," in IEEE Transactions on Industrial Electronics, vol. 65, no. 3, pp. 2817-2827, March 2018, doi: 10.1109/TIE.2017.2745407.

[4] Radford, N.A., Strawser, P., Hambuchen, K., Mehling, J.S., Verdeyen, W.K., Donnan, A.S, et al. (2015), Valkyrie: NASA's First Bipedal Humanoid Robot. J. Field Robotics, 32: 397-419. https://doi.org/10.1002/rob.21560.

[5] Gill Andrews Pratt, Low Impedance Walking Robots, Integrative and Comparative Biology, Volume 42, Issue 1, February 2002, Pages 174–181, https://doi.org/10.1093/icb/42.1.174

[6] M. A. Diftler et al., "Robonaut 2 - The first humanoid robot in space," 2011 IEEE International Conference on Robotics and Automation, Shanghai, China, 2011, pp. 2178-2183, doi: 10.1109/ICRA.2011.5979830.,

[7] W. Roozing, J. Malzahn, N. Kashiri, D. G. Caldwell and N. G. Tsagarakis, "On the Stiffness Selection for Torque-Controlled Series-Elastic Actuators," in IEEE Robotics and Automation Letters, vol. 2, no. 4, pp. 2255-2262, Oct. 2017, doi: 10.1109/LRA.2017.2726141.,

[8] Wyeth, Gordon. "Control issues for velocity sourced series elastic actuators." Proceedings of the 2006 Australasian Conference on Robotics and Automation. Australian Robotics and Automation Association, 2006.